

ON THE DISPERSION RELATIONS OF TAPERED CORE OPTICAL FIBERS WITH LIQUID CRYSTAL CLAD

P. K. Choudhury^{1,*} and P. T. S. Ping²

¹Institute of Microengineering and Nanoelectronics (IMEN), Universiti Kebangsaan Malaysia, 43600 UKM, Bangi, Selangor, Malaysia

²Hitachi Cable Asia Pacific Pte. Ltd., Mines Waterfront Business Park, No. 3, Jalan Tasik, 43300 Seri Kembangan, Selangor, Malaysia

Abstract—The paper deals with the case of a three-layer liquid crystal tapered optical fiber (LCTOF) for which the dispersion relations are deduced corresponding to the TE and the TM modes. For the LCTOF under consideration, the outermost clad section is made of liquid crystal material with radial anisotropy whereas the core and the inner clad are homogeneous, non-magnetic and isotropic dielectric regions. Rigorous field expressions corresponding to different LCTOF sections are deduced, and the eigenvalue equations are reported followed by the modal behaviour of the guide in respect of the propagation constants and cutoff situations. Apart from that, a glimpse of the power confinement through the TE and the TM excitations in different fiber sections is also touched upon.

1. INTRODUCTION

Liquid crystal optical fibers (LCOFs) [1–3] fall into the category of complex waveguides [4–17] that possess several technological applications. Optical applications of liquid crystals lie in their presenting the property of fairly large polarization anisotropy [18], which makes the fibers made of such materials much attractive among the relevant R&D community. Further, since liquid crystals exhibit very large electro-optic coefficient), the macroscopic optical properties of them can be manipulated by suitably applying external electrical fields — the phenomenon much useful in optical sensing applications [18, 19].

Received 24 May 2011, Accepted 16 June 2011, Scheduled 24 June 2011

* Corresponding author: Pankaj Kumar Choudhury (pankaj@ukm.m).

Among the radial and azimuthal anisotropies in LCOFs, studies of the latter type have appeared in the literature [20–22]. However, radially anisotropic LCOFs [23] are not given that much emphasis; it may be obtained by the capillary action after inserting the liquid crystal section into a capillary tube coated with N, N-dimethyl-N-octadecyl-3-aminopropyltrimethoxysilyl chloride. The present investigation is pivoted to the discussion of a three-layer LCOF where the outermost cladding section is composed of radially anisotropic liquid crystal material. The fiber core and the inner clad regions are isotropic dielectrics. Further, a tapered structure of the fiber core is taken into account along the longitudinal direction keeping in view that tapered fibers are of immense use in optical sensors and other in-line integrated optic applications [24–30]. As such, an amalgamation of features in respect of fiber geometry and the material, i.e., a tapered core fiber with radially anisotropic outermost liquid crystal clad, would provide enhanced usefulness of the guide.

The present communication aims at the investigation of the dispersion relations of the liquid crystal tapered optical fiber (LCTOF) structure for which Maxwell's equations are implemented for a rigorous analysis. Illustrations are made of the dispersion profile corresponding to the low order TE and TM modes, and the modal propagation constants are determined. This is to be added at this point that, though the studies related to radially anisotropic LCOFs have been reported before by Choudhury and Yoshino [31], the present study provides a blend of liquid crystal material and tapered structure wherein, apart from the propagation behaviour of the guide in terms of mode cutoffs, a superficial look at the power confinement factors [31] is also given in order to emphasize the usefulness of the guide.

2. THEORY

Figure 1 depicts the cross-section of LCTOF made of homogeneous, isotropic and non-magnetic core and the inner clad; the infinitely extended outer clad (the shaded region) consists of radially anisotropic liquid crystal material. In this figure, the dashed lines in the outer clad represent the elongation of the liquid crystal molecules. The tapered nature of the fiber cross-section becomes explicit from its longitudinal view (Fig. 2). The core and the inner clad sections have the refractive index (RI) values as n_1 and n_2 , respectively, with $n_1 > n_2$. Also, we consider radial elongation of the liquid crystal molecules in the infinitely extended outer clad with the ordinary and the extraordinary RI values as n_o and n_e , respectively.

We implement the cylindrical polar coordinate system (ρ, ϕ, z)

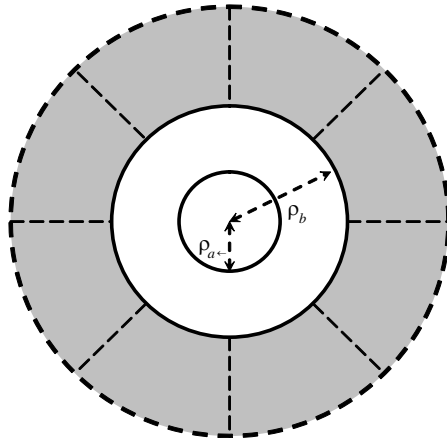


Figure 1. Cross-sectional view of LCTOF with the nematic liquid crystal outer clad.

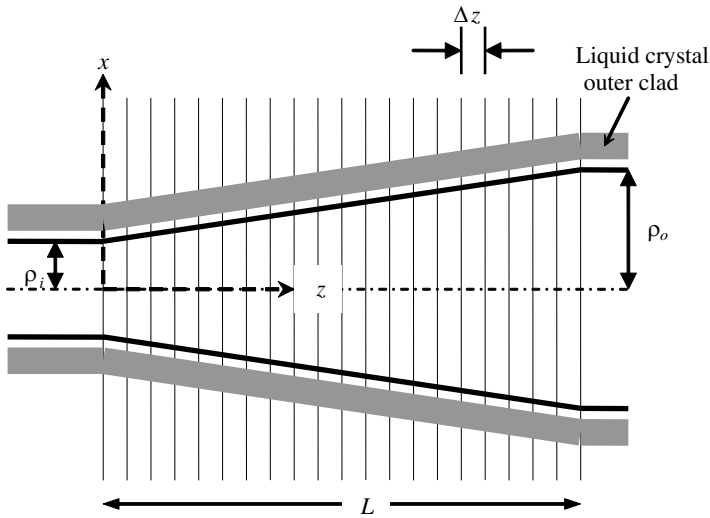


Figure 2. Longitudinal view of the LCTOF of length L .

wherein the z -axis remains along the direction of propagation and coincides with the principal axes of the outer clad. The extraordinary principal axis has a radial orientation, and therefore, the infinitely extended outer clad possesses the RI distribution as

$$n_\rho = n_e \quad \text{and} \quad n_\phi = n_z \quad \text{with} \quad n_e > n_1 > n_2 > n_o,$$

as depicted Figs. 3(a) and 3(b).

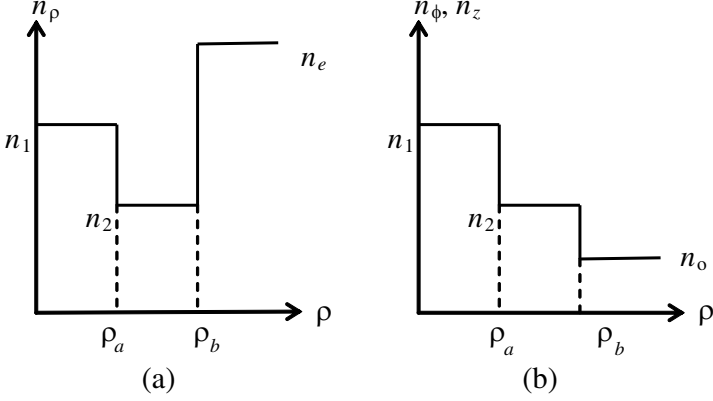


Figure 3. The RI distribution pattern.

The linear taper nature of the fiber core, as illustrated in Fig. 2, is defined through considering the taper radius as a function of z , i.e., $\rho(z)$, as [30]

$$\rho(z) = \rho_i - \frac{z}{L} (\rho_i - \rho_o) \quad (1)$$

where ρ_i and ρ_o , respectively, represent the radius of the input and the output ends of the tapered fiber of length L . In Fig. 2, the region with $z < z_i (= 0)$ corresponds to the fiber pigtail, and those with $z > z_o (= L)$ to the expanded cylindrical section.

Considering the time t -harmonic and the axis z -harmonic electromagnetic (EM) fields, coupled wave propagation equations for the transverse field components can be written as [31]

$$\begin{aligned} & \left(\nabla_t^2 + k_0^2 n_\rho^2 - \beta^2 - \frac{1}{\rho^2} \right) e_\rho \\ &= -\frac{2}{\rho^2} \frac{\partial e_\phi}{\partial \phi} + \left(1 - \frac{n_\rho^2}{n_z^2} \right) \frac{\partial}{\partial \rho} \left\{ \frac{1}{\rho} \frac{\partial}{\partial \rho} (\rho e_\rho) \right\} + \left(1 - \frac{n_\phi^2}{n_z^2} \right) \frac{\partial}{\partial \rho} \left(\frac{1}{\rho} \frac{\partial e_\phi}{\partial \phi} \right) \end{aligned} \quad (2a)$$

$$\begin{aligned} & \left(\nabla_t^2 + k_0^2 n_\phi^2 - \beta^2 - \frac{1}{\rho^2} \right) e_\phi \\ &= \frac{2}{\rho^2} \frac{\partial e_\rho}{\partial \phi} + \frac{1}{\rho^2} \left\{ \left(1 - \frac{n_\rho^2}{n_z^2} \right) \frac{\partial}{\partial \rho} \left(\rho \frac{\partial e_\rho}{\partial \phi} \right) + \left(1 - \frac{n_\phi^2}{n_z^2} \right) \frac{\partial^2 e_\phi}{\partial \phi^2} \right\} \end{aligned} \quad (2b)$$

In Eqs. (2), ∇_t^2 is the Laplacian operator in the cylindrical coordinate system, k_0 is the free-space propagation constant, and n_ρ ,

n_ϕ and n_z are, respectively, the RI values along the ρ -, ϕ - and z -directions. Further, β -values in Eqs. (2) are governed by a Taylor series expansion [28], i.e.,

$$\beta = \beta_0 + \left(\frac{\partial \beta}{\partial z} \right) z, \quad (3)$$

owing to the variation of the propagation constant β due to the varying cross-sectional dimension with distance z . In Eq. (3), the higher order terms are suppressed during the expansion as the results will not be affected much, and β_0 is the axial component of the propagation vector at the origin $z = 0$.

We consider the lower order TE and TM modes, viz. TE_{01} and TM_{01} . For the TE_{01} mode, there exists only one transverse electrical field component e_ϕ , which is independent of the coordinate ϕ , making thereby $e_\rho = 0$ and $\partial e_\phi / \partial \phi = 0$ for this type of mode. For the TM_{01} mode, there is only one non-zero component e_ρ , which is independent of the coordinate ϕ , and therefore, one can have $e_\phi = 0$ and $\partial e_\rho / \partial \phi = 0$.

Following Eqs. (2) and the above described condition for the TE_{01} mode, it can be shown that the EM field components in this case will be ultimately given as follows:

Core region:

$$H_\rho)_I = -A_{\phi 1} \frac{\beta}{\omega \mu_0} J_1(\gamma_1 \rho) \exp \{j(\omega t - \beta z)\} \quad (4a)$$

$$H_z)_I = A_{\phi 1} \frac{j}{\omega \mu_0} \left\{ \gamma_1 J_1'(\gamma_1 \rho) + \frac{1}{\rho} J_1(\gamma_1 \rho) \right\} \exp \{j(\omega t - \beta z)\} \quad (4b)$$

Inner clad region:

$$H_\rho)_II = -\frac{\beta}{\omega \mu_0} \{A_{\phi 2} K_1(\gamma_2 \rho) + A_{\phi 3} I_1(\gamma_2 \rho)\} \exp \{j(\omega t - \beta z)\} \quad (5a)$$

$$H_z)_II = \frac{j}{\omega \mu_0} \left[A_{\phi 2} \left\{ \gamma_2 K_1'(\gamma_2 \rho) + \frac{1}{\rho} K_1(\gamma_2 \rho) \right\} + A_{\phi 3} \left\{ \gamma_2 I_1'(\gamma_2 \rho) + \frac{1}{\rho} I_1(\gamma_2 \rho) \right\} \right] \exp \{j(\omega t - \beta z)\} \quad (5b)$$

Outer clad region:

$$H_\rho)_III = -A_{\phi 4} \frac{\beta}{\omega \mu_0} K_1(\gamma_3 \rho) \exp \{j(\omega t - \beta z)\} \quad (6a)$$

$$H_z)_III = A_{\phi 4} \frac{j}{\omega \mu_0} \left\{ \gamma_3 K_1'(\gamma_3 \rho) + \frac{1}{\rho} K_1(\gamma_3 \rho) \right\} \exp \{j(\omega t - \beta z)\} \quad (6b)$$

In Eqs. (4), (5) and (6), μ_0 is the free-space permeability and ω is the angular frequency of the unbounded medium. $J(\cdot)$, $K(\cdot)$ and

$I(\cdot)$ represent Bessel and the modified Bessel functions, and prime stands for the differentiation with respect to the argument of the function. Also, $A_{\phi 1}$, $A_{\phi 2}$, $A_{\phi 3}$ and $A_{\phi 4}$ are the arbitrary constants to be determined by the boundary conditions, and the quantities γ_1 , γ_2 and γ_3 are defined as

$$\gamma_1 = \sqrt{n_1^2 k_0^2 - \beta^2} \quad (7a)$$

$$\gamma_2 = \sqrt{\beta^2 - n_2^2 k_0^2} \quad (7b)$$

$$\gamma_3 = \sqrt{\beta^2 - n_o^2 k_0^2} \quad (7c)$$

It is to be remembered that ρ and β are governed by Eqs. (1) and (3), respectively.

For the sake of simplicity, localized values of the radial parameters of LCTOF are considered to determine the interfaces. In this stream, we match the fields at the interfaces $\rho = \rho_a$ (core-inner clad interface) and $\rho = \rho_b$ (inner clad-outer clad interface), where ρ_a and ρ_b , respectively, determine the local parametric values of the LCTOF core and the inner clad radii. After matching the fields at the layer boundaries, and collecting the coefficients of the unknown arbitrary constants, the following 4×4 matrix can be obtained after a few lengthy steps:

$$\begin{pmatrix} \xi_{11} & -\xi_{12} & -\xi_{13} & 0 \\ 0 & \xi_{22} & \xi_{23} & -\xi_{24} \\ \xi_{31} & -\xi_{32} & -\xi_{33} & 0 \\ 0 & \xi_{42} & \xi_{43} & -\xi_{44} \end{pmatrix} = \Delta_{TE}(\text{say}) = 0 \quad (8)$$

Various symbols in this equation have their meanings as follows:

$$\xi_{11} = (\beta/\omega\mu_0) J_\nu(u\rho_a) e^{\{j(\omega t - \beta z)\}}, \quad \xi_{12} = (\beta/\omega\mu_0) K_\nu(w\rho_a) e^{\{j(\omega t - \beta z)\}},$$

$$\xi_{13} = (\beta/\omega\mu_0) I_\nu(w\rho_a) e^{\{j(\omega t - \beta z)\}}, \quad \xi_{14} = (\beta/\omega\mu_0) K_\nu(w\rho_b) e^{\{j(\omega t - \beta z)\}},$$

$$\xi_{23} = (\beta/\omega\mu_0) I_\nu(w\rho_b) e^{\{j(\omega t - \beta z)\}}, \quad \xi_{24} = (\beta/\omega\mu_0) K_\nu(v\rho_b) e^{\{j(\omega t - \beta z)\}},$$

$$\xi_{31} = (j/\omega\mu_0) \{uJ'_\nu(u\rho_a) + (1/\rho_a) J_\nu(u\rho_a)\} e^{\{j(\omega t - \beta z)\}},$$

$$\xi_{32} = (j/\omega\mu_0) \{wK'_\nu(w\rho_a) + (1/\rho_a) K_\nu(w\rho_a)\} e^{\{j(\omega t - \beta z)\}},$$

$$\xi_{33} = (j/\omega\mu_0) \{wI'_\nu(w\rho_a) + (1/\rho_a) I_\nu(w\rho_a)\} e^{\{j(\omega t - \beta z)\}},$$

$$\xi_{42} = (j/\omega\mu_0) \{wK'_\nu(w\rho_b) + (1/\rho_b) K_\nu(w\rho_b)\} e^{\{j(\omega t - \beta z)\}},$$

$$\xi_{43} = (j/\omega\mu_0) \{wI'_\nu(w\rho_b) + (1/\rho_b) I_\nu(w\rho_b)\} e^{\{j(\omega t - \beta z)\}},$$

$$\text{and } \xi_{44} = (j/\omega\mu_0) \{vK'_\nu(v\rho_b) + (1/\rho_b) K_\nu(v\rho_b)\} e^{\{j(\omega t - \beta z)\}}.$$

The above Eq. (8) represents the dispersion relation for the LCTOF in the case of TE mode excitation. As such, the solutions to

this equation will provide different TE modes existing in the anisotropic fiber. Further, solving Eq. (8) under the condition $\omega^2 \rightarrow 0$ will provide the cutoff characteristics of the fiber under consideration.

We now move toward the TM mode excitation. Since $e_\phi = 0$ and $\partial e_\rho / \partial \phi = 0$ in the case of TM_{01} mode, following Eqs. (2), it can be shown that the EM field components will be represented in this case as follows:

Core region:

$$E_z)_I = -B_{\rho 1} \frac{j}{\beta \eta} \left\{ \gamma_1 J_1'(\gamma_1 \rho) + \frac{1}{\rho} J_1(\gamma_1 \rho) \right\} \exp \{j(\omega t - \beta z)\} \quad (9a)$$

$$H_\phi)_I = B_{\rho 1} \frac{\omega \epsilon_0}{\beta} n_\rho^2 J_1(\gamma_1 \rho) \exp \{j(\omega t - \beta z)\} \quad (9b)$$

Inner clad region:

$$E_z)_{II} = -\frac{j}{\beta \eta} \left[B_{\rho 2} \left\{ \gamma_2 K_1'(\gamma_2 \rho) + \frac{1}{\rho} K_1(\gamma_2 \rho) \right\} + B_{\rho 3} \left\{ \gamma_2 I_1'(\gamma_2 \rho) + \frac{1}{\rho} I_1(\gamma_2 \rho) \right\} \right] \exp \{j(\omega t - \beta z)\} \quad (10a)$$

$$H_\phi)_{II} = \frac{\omega \epsilon_0}{\beta} n_\rho^2 \{B_{\rho 2} K_1(\gamma_2 \rho) + B_{\rho 3} I_1(\gamma_2 \rho)\} \exp \{j(\omega t - \beta z)\} \quad (10b)$$

Outer clad region:

$$E_z)_{III} = -B_{\rho 4} \frac{j}{\beta \eta} \left\{ \gamma_3' K_1'(\gamma_3' \rho) + \frac{1}{\rho} K_1(\gamma_3' \rho) \right\} \exp \{j(\omega t - \beta z)\} \quad (11a)$$

$$H_\phi)_{III} = B_{\rho 4} \frac{\omega \epsilon_0}{\beta} n_\rho^2 K_1(\gamma_3' \rho) \exp \{j(\omega t - \beta z)\} \quad (11b)$$

In Eqs. (9), (10) and (11), $B_{\rho 1}$, $B_{\rho 2}$, $B_{\rho 3}$ and $B_{\rho 4}$ are arbitrary constants to be defined by the boundary conditions, and the new quantities η and γ_3' have the meanings as

$$\eta = (n_0/n_e)^2 \quad (12)$$

$$\gamma_3' = \frac{n_o}{n_e} \sqrt{n_e^2 k_0^2 - \beta^2} \quad (13)$$

Now, following the procedure as discussed above for the case of TE modes, matching of the EM field components at the localized radial parameters of the LCTOF, i.e., $\rho = \rho_a$ (core-inner clad interface) and $\rho = \rho_b$ (inner clad-outer clad interface), will ultimately yield (after collecting the coefficients of the unknown constants) the following eigenvalue equation in the form of 4×4 matrix:

$$\begin{pmatrix} \zeta_{11} & -\zeta_{12} & -\zeta_{13} & 0 \\ 0 & \zeta_{22} & \zeta_{23} & -\zeta_{24} \\ \zeta_{31} & -\zeta_{32} & -\zeta_{33} & 0 \\ 0 & \zeta_{42} & \zeta_{43} & -\zeta_{44} \end{pmatrix} = \Delta_{TM}(\text{say}) = 0 \quad (14)$$

Equation (14) is the dispersion relation for the LCTOF in the case of TM modes with the symbols having their meanings as follows:

$$\begin{aligned}
\zeta_{11} &= (j/\beta\eta^2) \{uJ'_\nu(u\rho_a) + (1/\rho_a) J_\nu(u\rho_a)\} e^{j(\omega t - \beta z)}, \\
\zeta_{12} &= (j/\beta\eta^2) \{wK'_\nu(w\rho_a) + (1/\rho_a) K_\nu(w\rho_a)\} e^{j(\omega t - \beta z)}, \\
\zeta_{13} &= (j/\beta\eta^2) \{wI'_\nu(w\rho_a) + (1/\rho_a) I_\nu(w\rho_a)\} e^{j(\omega t - \beta z)}, \\
\zeta_{22} &= (j/\beta\eta^2) \{wK'_\nu(w\rho_b) + (1/\rho_b) K_\nu(w\rho_b)\} e^{j(\omega t - \beta z)}, \\
\zeta_{23} &= (j/\beta\eta^2) \{wI'_\nu(w\rho_b) + (1/\rho_b) I_\nu(w\rho_b)\} e^{j(\omega t - \beta z)}, \\
\zeta_{24} &= (j/\beta\eta^2) \{vK'_\nu(v\rho_b) + (1/\rho_b) K_\nu(v\rho_b)\} e^{j(\omega t - \beta z)}, \\
\zeta_{31} &= (\omega\varepsilon_0/\beta) n_\rho^2 J_\nu(u\rho_a) e^{j(\omega t - \beta z)}, \\
\zeta_{32} &= (\omega\varepsilon_0/\beta) n_\rho^2 K_\nu(w\rho_a) e^{j(\omega t - \beta z)}, \\
\zeta_{33} &= (\omega\varepsilon_0/\beta) n_\rho^2 I_\nu(w\rho_a) e^{j(\omega t - \beta z)}, \\
\zeta_{42} &= (\omega\varepsilon_0/\beta) n_\rho^2 K_\nu(u\rho_a) e^{j(\omega t - \beta z)}, \\
\zeta_{43} &= (\omega\varepsilon_0/\beta) n_\rho^2 I_\nu(w\rho_b) e^{j(\omega t - \beta z)} \\
\text{and } \zeta_{44} &= (\omega\varepsilon_0/\beta) n_\rho^2 K_\nu(v\rho_b) e^{j(\omega t - \beta z)}.
\end{aligned}$$

Equation (14) provides the dispersion relation (or the eigenvalue relation) for the LCTOF in the case of TM mode excitation. The solutions to this equation will, therefore, yield different TM modes existing in the anisotropic guide, and also, solving this equation under the condition $w^2 \rightarrow 0$ will provide the cutoff characteristics of the fiber under consideration.

3. RESULTS AND DISCUSSION

Equations (8) and (14), corresponding to the TE and the TM mode excitations, respectively, constitute the central new results of this analytical investigation. In this context, the authors wish to point out that the tapered core dielectric optical fiber itself is a complex problem to tackle analytically. The radial anisotropy of liquid crystal material in the outermost clad section adds further complexities. It may be concluded that this analysis has been brought to a point where the characteristic equations involve Bessel and the modified Bessel functions, which the authors understand as a good starting point for the study of such anisotropic tapered guides with elliptical cores — the guides that would be more applicable in sensing as well as mode discrimination. However, this analysis is out of the scope of the present paper, and is expected to be taken up in a future communication.

We are now in a position to analyze the characteristics of LCTOFs in respect of their dispersion behaviour and field cutoffs corresponding to the cases of TE and TM mode excitations. It is rather known that, in the case of isotropic guides, TE and TM modes are difficult to separate because the direction independent RI values yield identical propagation constants and field cutoffs. However, the TE and the TM modes undergo different polarizations in the case of anisotropic guides (such as liquid crystal waveguides) owing to the direction dependent RIs, and therefore, these modes possess different values of propagation constants and field cutoffs.

As stated above, our LCTOF structure has three different sections (i.e., three-layer step-index optical fiber) with radially anisotropic liquid crystal outer clad. The RI values of the core and the inner clad are considered to be $n_1 = 1.5$ and $n_2 = 1.46$, respectively. Further, in our illustrative case, for the outermost section, we used nematic liquid crystal as BDH mixture 14616, which has the respective ordinary and extraordinary RI values as $n_o = 1.457$ and $n_e = 1.5037$. For simplicity, we considered the lower order modes with the azimuthal index (ν) values as 1, 2 and 3. The taper length L in all the computations is taken to be 5 cm, the localized values of the core and the inner clad radii are considered as $60 \mu\text{m}$ and $120 \mu\text{m}$, respectively, and the operating wavelength is kept fixed at $1.55 \mu\text{m}$.

Figure 4(a) illustrates the plots of the left hand side of the dispersion relation represented by Eq. (8) corresponding to the case of TE mode excitation for three different values of ν as stated above. The intersection of the curves with the horizontal axis (i.e., the zero crossings of the curves) represents the existence of modes with a particular value of the propagation constant β . We observe that the propagation constant of the first mode corresponding to $\nu = 1$ has a value close to $5.935 \times 10^6 \text{ m}^{-1}$, and the values of zero crossings slightly increase with the increase in the azimuthal index. The propagation constants of the other existing modes can also be estimated from the zero crossings of the curves. The cutoff characteristics of the TE modes can be obtained after solving Eq. (8) under the limiting condition $w^2 \rightarrow 0$. In this situation, the graphs are plotted in Fig. 4(b) (the $(\text{TE})_{\text{Cutoff}}$ vs. β plots), and we notice that the zero crossings of the curves indicate lesser cutoff β -values (for $\nu = 1$, the cutoff β -value is close to $5.918 \times 10^6 \text{ m}^{-1}$) than the β -values of the first existing mode, when compared with the corresponding plots of Fig. 4(a). This essentially indicates the consistency of the results illustrated through Figs. 4(a) and 4(b).

Results corresponding to the TM modes are illustrated in Figs. 5(a) and 5(b). Fig. 5(a) shows the plots of the left hand side

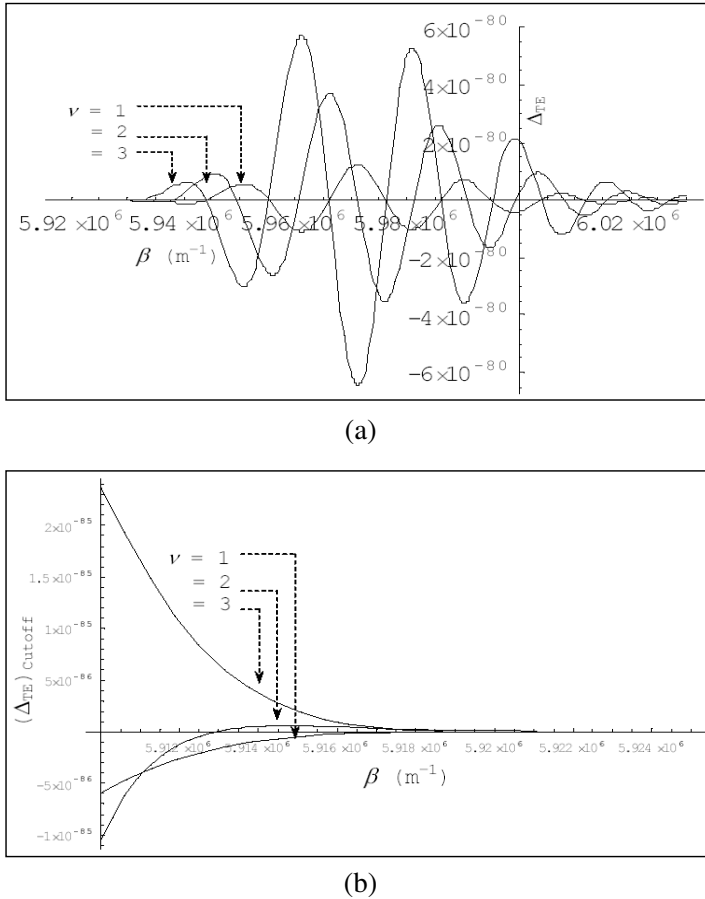
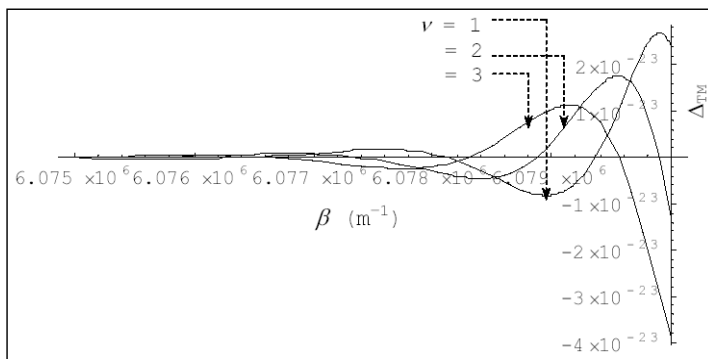
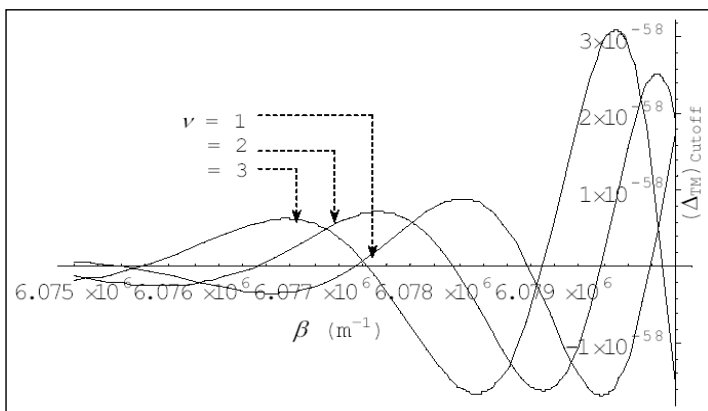


Figure 4. (a) Plot of the dispersion relation for the TE modes. (b) Plot of the cutoff characteristics for the TE modes.

of the dispersion relation represented by Eq. (14) whereas Fig. 5(b) corresponds to the cutoff plots of Eq. (14) under the limiting condition $w^2 \rightarrow 0$. We take the azimuthal index (ν) values as 1, 2 and 3. As stated above, the zero crossings of the curve with the β -axis represents the existence of a mode. We observe from Fig. 5(a) that the value of the propagation constant for the first mode corresponding to $\nu = 1$ exists around $\beta = 6.076 \times 10^6 \text{ m}^{-1}$, which is smaller than that correspondingly observed zero crossing in the case of TE modes. As such, in the case of TM modes, the β -values show a substantial decrease as compared to the TE modes. Further, with the increase in azimuthal index, the β -values have a tendency to increase, which is similar to the situation



(a)



(b)

Figure 5. (a) Plot of the dispersion relation for the TM modes. (b) Plot of the cutoff characteristics for the TM modes.

observed in the case of TE modes. In this case too, the propagation constants of the other modes existing in the guide can be estimated from the zero crossings of the curves. As to the cutoff values in the case of TM modes, as observed from Fig. 5(b) (i.e., the $(\Delta_{TM})_{\text{Cutoff}}$ vs. β plots), the first zero crossings of the curves exist earlier than those seen in the corresponding plots in Fig. 5(a), indicating thereby the consistency of the results presented in Figs. 5(a) and 5(b). The only noticeable fact observed is that the TE eigenmodes propagate in the aforesaid anisotropic guide with larger propagation constants as compared to the TM eigenmodes.

Along with the propagation constants and the cutoff situations of the different existing modes, it would be rather interesting to get

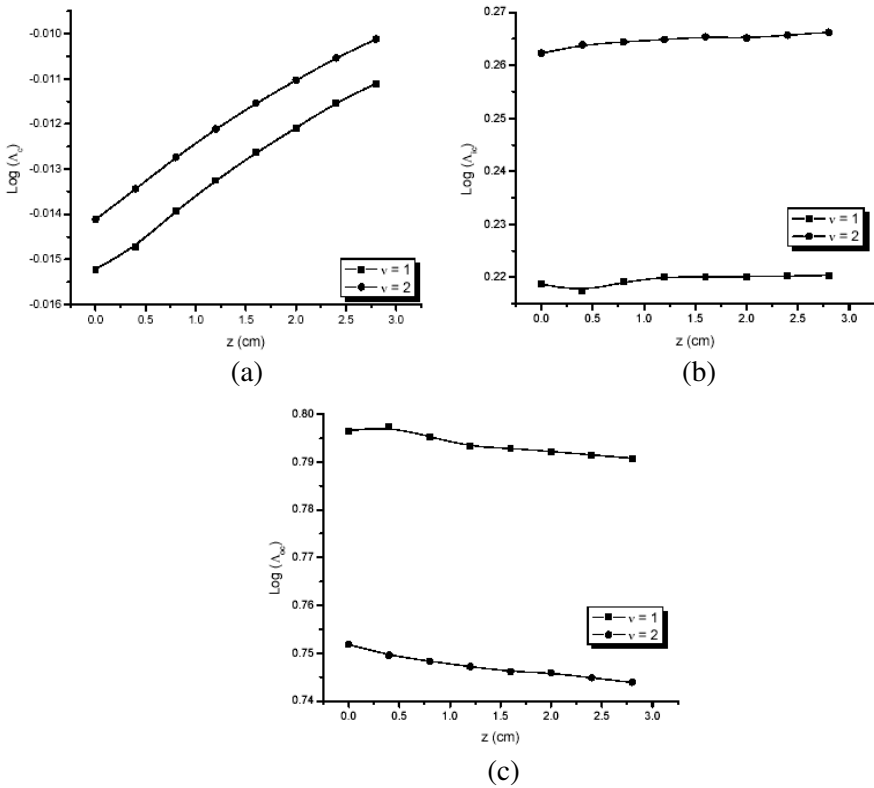


Figure 6. Plot of the power confinement factors in the LCTOF (a) core, (b) the inner clad and (c) the outer clad regions under the TE mode excitation.

a glimpse of the characteristics of the propagation of power through the anisotropic guide. The expression of power in the different fiber sections may be easily deduced by implementing the field components (as obtained in Section 2) and the Poynting vector [32]. These expressions are not explicitly shown here owing to their lengthy forms, and may be found in Ref. [29]. Figs. 6 and 7, respectively, illustrate the logarithmic plots of the confinement of power against the taper length in the cases of TE and TM modes. In these figures, Λ_c , Λ_{ic} and Λ_{oc} represent the confinement factors in the fiber core, inner clad and the outer clad sections. For the computation purpose, the operating wavelength is kept fixed at $1.55 \mu\text{m}$. Also, the LCTOF core radii at the input and the output ends are kept fixed as $50 \mu\text{m}$ and $100 \mu\text{m}$, respectively, and two lower azimuthal index values are taken, i.e., $\nu = 1, 2$.

At this point, it is worth to make explicit the definition of power confinement factor [31]. In a region of guide, it is the ratio of the power sustained in that particular region to the total amount of power transported by (all the sections of) the guide. As such, Λ_c represents the ratio of the amount of power that is being propagated in the LCTOF core to the total power transmitted by the LCTOF. The explicit meanings of Λ_{ic} and Λ_{oc} can also be extracted in this way.

Figures 6(a), 6(b) and 6(c), respectively, represent the power transported by the TE modes in the core, inner clad and the outer clad sections along the longitudinal length of the taper. We observe that there is a gradual increase of power with the taper length in the fiber core, becomes almost uniform with a substantial increase in the inner clad section, and the outermost clad sustains the maximum amount of power. Further, in all the cases, the modes with higher azimuthal index carry higher amount of power. Looking at the power confinements in

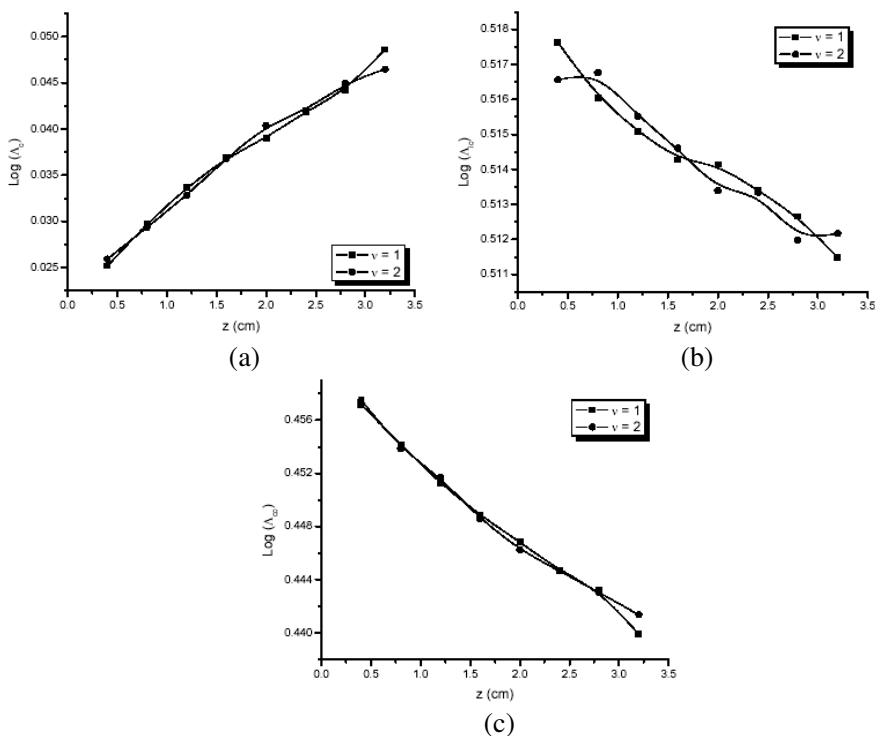


Figure 7. Plot of the power confinement factors in the LCTOF (a) core, (b) the inner clad and (c) the outer clad regions under the TM mode excitation.

all the three sections, the noticeable fact is that, with the decrease of power in the fiber core and/or the inner clad, it simultaneously increases in the outermost liquid crystal clad, indicating thereby as if the power is *leaking off* the fiber core, and propagating through the clad sections. This is essentially attributed to the presence of liquid crystal in the outermost region of the fiber. This enhancement of power in the outer region would be of much use for the purpose of optical sensing as well as field coupling.

Figures 7(a), 7(b) and 7(c) depict the power transported by the TM modes in the core, inner clad and the outer clad sections, respectively, of the guide. We observe that, TM field excitation does not make a prominent increase in power in the outermost liquid crystal clad — the phenomenon observed in the case of TE mode excitation. We notice that the highest amount of power is sustained in the inner clad region, and the confinement factor in the outermost clad is slightly less than that in the inner clad; the minimum amount of power remains confined in the fiber core.

4. CONCLUSION

The foregoing discussion focuses on the dispersion characteristics of the radially anisotropic LCTOF and their power confinement factors corresponding to the TE and TM mode excitations. It is found that the TE eigenmodes propagate in the guide with larger propagation constants as compared to the TM eigenmodes. Also, the TE mode excitation essentially makes enough power available in the liquid crystal clad region for the usage of the guide in optical sensing and/or directional coupling. This interesting feature is attributed to the incorporation of the radially anisotropic liquid crystal material in the outermost clad region.

ACKNOWLEDGMENT

The authors are grateful to the two anonymous reviewers for constructive criticisms on the manuscript. One of the authors (PKC) is thankful to Prof. Burhanuddin Yeop Majlis for constant encouragement and help. Fruitful suggestions by Prof. S. Shaari are also gratefully acknowledged.

REFERENCES

1. Veilleux, C., J. Lapierre, and J. Bures, "Liquid-crystal-clad tapered fibers," *Opt. Lett.*, Vol. 11, 733–735, 1986.

2. Green, M. and S. J. Madden, "Low loss nematic liquid crystal cored fiber waveguides," *Appl. Opt.*, Vol. 28, 5202–5203, 1989.
3. Lin, H., P. P. Muhoray and M. A. Lee, "Liquid crystalline cores for optical fibers," *Mol. Cryst. Liq. Cryst.*, Vol. 204, 189–200, 1991.
4. Kumar, D., P. K. Choudhury, and O. N. Singh, II, "Towards the dispersion relations for dielectric optical fibers with helical windings under slow- and fast-wave considerations — a comparative analysis," *Progress In Electromagnetics Research*, Vol. 80, 409–420, 2008.
5. Safie, A. H. B. M. and P. K. Choudhury, "On the field patterns of helical clad dielectric optical fibers," *Progress In Electromagnetics Research*, Vol. 91, 69–84, 2009.
6. Siong, C. C. and P. K. Choudhury, "Propagation characteristics of tapered core helical clad dielectric optical fibers," *Journal of Electromagnetic Waves and Applications*, Vol. 23, Nos. 5–6, 663–674, 2009.
7. Abd-Rahman, F., P. K. Choudhury, D. Kumar, and Z. Yusoff, "An analytical investigation of four-layer dielectric optical fibers with Au nano-coating — A comparison with three-layer optical fibers," *Progress In Electromagnetics Research*, Vol. 90, 269–286, 2009.
8. Choudhury, P. K. and D. Kumar, "On the slow-wave helical clad elliptical fibers," *Journal of Electromagnetic Waves and Applications*, Vol. 24, Nos. 14–15, 1931–1942, 2010.
9. Amin, A. S. N., M. Mirhosseini, and M. Shahabadi, "Modal analysis of multilayer conical dielectric waveguides for azimuthal invariant modes," *Progress In Electromagnetics Research*, Vol. 105, 213–229, 2010.
10. Chen, D. and B. Sun, "Multi-wavelength fiber optical parametric oscillator based on a highly nonlinear fiber and a sagnac loop filter," *Progress In Electromagnetics Research*, Vol. 106, 163–176, 2010.
11. Tuz, V. R. and C.-W. Qiu, "Semi-infinite chiral nihility photonics: Parametric dependence, wave tunneling and rejection," *Progress In Electromagnetics Research*, Vol. 103, 139–152, 2010.
12. Ahmed, S. and Q. A. Naqvi, "Electromagnetic scattering from a chiral-coated nihility cylinder," *Progress In Electromagnetics Research Letters*, Vol. 18, 41–50, 2010.
13. Baqir, M. A., A. A. Syed, and Q. A. Naqvi, "Electromagnetic fields in a circular waveguide containing chiral nihility metamaterial," *Progress In Electromagnetics Research M*, Vol. 16, 85–93, 2011.

14. Kesari, V. and J. P. Keshari, "Analysis of a circular waveguide loaded with dielectric and metal discs," *Progress In Electromagnetics Research*, Vol. 111, 253–269, 2011.
15. Dong, J., J. Li, and F.-Q. Yang, "Guided modes in the four-layer slab waveguide containing chiral nihility core," *Progress In Electromagnetics Research*, Vol. 112, 241–255, 2011.
16. Petrillo, L., F. Jangal, M. Darces, J.-L. Montmagnon, and M. Helier, "Negative permittivity media able to propagate a surface wave," *Progress In Electromagnetics Research*, Vol. 115, 1–10, 2011.
17. Liu, S.-H. and L.-X. Guo, "Negative refraction in an anisotropic metamaterial with a rotation angle between the principal axis and the planar interface," *Progress In Electromagnetics Research*, Vol. 115, 243–257, 2011.
18. Wu, S.-T. and U. Efron, "Optical properties of thin nematic liquid crystal cells," *Appl. Phys. Lett.*, Vol. 48, 624–636, 1986.
19. Goldburt, E. S. and P. S. J. Russell, "Electro-optical response of a liquid-crystalline fiber coupler," *Appl. Phys. Lett.*, Vol. 48, 10–12, 1986.
20. Sage, I. and D. Chaplin, "Low RI liquid crystals for integrated optics," *Electron. Lett.*, Vol. 23, 1192–1193, 1987.
21. Kashyap, R., C. S. Winter, and B. K. Nayar, "Polarization desensitized liquid-crystal overlay optical-fiber modulator," *Opt. Lett.*, Vol. 13, 401–403, 1988.
22. Ioannidis, Z. K., I. P. Giles, and C. Bowry, "All-fiber optic intensity modulators using liquid crystals," *Appl. Opt.*, Vol. 30, 328–333, 1991.
23. Chen, S.-H. and T.-J. Chen, "Observation of mode selection in a radially anisotropic cylindrical waveguide with liquid-crystal cladding," *Appl. Phys. Lett.*, Vol. 64, 1893–1895, 1994.
24. Black, R. J., F. Gonthier, S. Lacroix, and J. D. Love, "Tapered single-mode fibres and devices: I. Adiabaticity criteria," *IEE Proc. — J.*, Vol. 138, 343–354, 1991.
25. Ono, K. and H. Osawa, "Excitation characteristics of fundamental mode in tapered slab waveguides with nonlinear cladding," *Electron. Lett.*, Vol. 27, 664–666, 1991.
26. Lim, M. H., S. C. Yeow, P. K. Choudhury, and D. Kumar, "Towards the dispersion characteristics of tapered core dielectric optical fibers," *Journal of Electromagnetic Waves and Applications*, Vol. 20, No. 12, 1597–1609, 2006.
27. Yeow, S. C., M. H. Lim, and P. K. Choudhury, "A rigorous

- analysis of the distribution of power in plastic clad linear tapered fibers,” *Optik*, Vol. 117, 405–410, 2006.
28. Choudhury, P. K. and D. Kumar, “Towards dispersion relations for tapered core dielectric elliptical fibers,” *Optik*, Vol. 118, 340–344, 2007.
 29. Choudhury, P. K. and W. K. Soon, “TE mode propagation through tapered core liquid crystal optical fibers,” *Progress In Electromagnetics Research*, Vol. 104, 449–463, 2010.
 30. Choudhury, P. K. and W. K. Soon, “On the transmission by liquid crystal tapered optical fibers,” *Optik*, Vol. 122, 1061–1068, 2011.
 31. Choudhury, P. K. and T. Yoshino, “TE and TM modes power transmission through liquid crystal optical fibers,” *Optik*, Vol. 115, 49–56, 2004.
 32. Cherin, A. H., *An Introduction to Optical Fibers*, Chapter 5, McGraw-Hill, New York, 1987.